IEEE Access
Multidisciplinary | Rapid Review | Open Access Journal

IEEE POWER & ENERGY SOCIETY SECTION

Received 17 August 2022, accepted 25 August 2022, date of publication 29 August 2022, date of current version 9 September 2022.

Digital Object Identifier 10.1109/ACCESS.2022.3202907

RESEARCH ARTICLE

Fractional Cascade LFC for Distributed Energy Sources via Advanced Optimization Technique Under High Renewable Shares

PAWAN KUMAR PATHAK[1], ANIL KUMAR YADAV[2], (Senior Member, IEEE), SANJEEVIKUMAR PADMANABAN[3], (Senior Member, IEEE), AND INNOCENT KAMWA[4], (Fellow, IEEE)

[1]School of Automation, Banasthali Vidyapith, Banasthali, Rajasthan 304022, India
[2]Department of Electrical Engineering, NIT Hamirpur, Hamirpur, Himachal Pradesh 177005, India
[3]Department of Electrical Engineering, Information Technology and Cybernetic, University of South-Eastern Norway, 3679 Notodden, Norway
[4]Department of Electrical and Computer Science Engineering, Laval University, Quebec City, QC G1V 0A6, Canada

Corresponding authors: Innocent Kamwa (innocent.kamwa@gel.ulaval.ca) and Pawan Kumar Pathak (ppathak999@gmail.com)

This work was supported by the Canada National Sciences and Engineering Research Council through the Laval University, Grant ALLRP567550-21.

ABSTRACT Unpredictable high renewable shares in a standalone microgrid (MG) system with stochastic load demands introduces an unavoidable mismatch among loads and sources. This mismatch directly impacts the system frequency, which can be mitigated via applying a suitable load frequency control (LFC) scheme. This brief proposes a maiden attempt of marine predator algorithm (MPA) assisted one plus proportional derivative with filter-fractional order proportional-integral ((1+PDF)-FOPI) controller to obtain the proper power flow management among loads and sources. The investigated MG system consists of a photovoltaic (PV) system, a wind turbine (WT) generator (WTG), and a diesel engine generator (DG) as the distributed energy sources, and an ultracapacitor (UC) and a flywheel are chosen as the energy storage elements (ESEs). Various system nonlinearities, such as governor dead-band (GDB) and generation rate constraint (GRC) are also considered to reflect the practical scenario. Five state-of-the-art optimization techniques and three traditional controllers, PID, FOPID, and PI-PD, are vividly compared to assess the proposed scheme's performance. The parametric uncertainties are considered obtaining the robust performance of the proposed control scheme. An eigenvalues-based stability evaluation of the considered plant employing the proposed LFC scheme is also included in this work. In the worst situation, the maximum frequency deviation is obtained as −0.016 Hz, which is entirely satisfactory and under the range of the IEEE standard. Finally, a modified New England IEEE-39 test bus system is chosen to perform the real power system validation via MATLAB/Simulink.

INDEX TERMS Microgrid, load frequency control, optimization technique, fractional cascade control, renewable energy sources, stability evaluation.

I. INTRODUCTION

A. BACKGROUND

Enhancing electricity demand requires employing hybrid generation units in standalone or interconnected power system networks. In the present era, renewable shares are enhancing the existing power system network due to the high emission of greenhouse gases, galloping oil prices, and sustainable development. Renewable energy (RE) sources, considered economical and clean energy sources, are likely to be interconnected to the MG power systems [1], [2]. Solar and wind are the most critical RE sources among all the energy sources due to their abundant availability [3]. The critical drawback of RE sources is their highly unpredictable nature.

The associate editor coordinating the review of this manuscript and approving it for publication was Okyay Kaynak.

Due to the stochastic nature of RE sources, its efficacy is very low; with PV, the conversion efficacy is as low as it falls under the range of 7-19% [3]. Hence, in order to harvest the maximum obtainable power from the uninterrupted solar insolation, various maximum power point tracking (MPPT) schemes are employed [3], [4], [5]. The most commonly utilized MPPT schemes are perturbed & observe (P&O) and incremental conductance (IC) [5]. With wind energy conversion, the most common MPPTs are P&O and tip speed ratio [6]. In this investigated MG system, the maximum obtainable power from PV is harvested through the modified IC (MIC) MPPT scheme as presented in [7], and a nonlinear WTG modeling is employed to harvest maximum power from the stochastic wind speed. Due to the significant share of these RE sources in the MG system, the most interesting parameter of the power system, ''frequency,'' is affected [8]. The change in frequency deviation (CFD) severely affects the frequency-sensitive loads, and in the worst situation, a blackout may occur. To maintain the proper power flow management among loads and sources and to make $CFD \rightarrow 0$, it is required to incorporate a supervisory LFC scheme in the MG system [9]. In other words, LFC allows the generating units to regulate their generations corresponding to load demands, resulting in a zero CFD under ideal situations. The system performance may undermine due to the improper design of LFC and also causing large oscillations in the system [10]. In order to the proper design of the LFC scheme, various meta-heuristics-based control approach is employed for various types of power system networks [7], [8]. The meta-heuristics handle the optimal performance of the designed frequency control scheme.

B. LITERATURE REVIEW

The apropos literature has witnessed various works on the novel controller design. Some of the recently published literature incorporates PI/PID structured controllers are dragonfly search algorithm [11], bacterial foraging optimization algorithm (BFOA) [12], particle swarm optimization (PSO) and hybrid BFOA (PSO-hBFOA) algorithm [13], lozi map-based chaotic algorithm [14], fire-fly algorithm tuned PI controller [15], PIDD2 control approach [16], ant colony optimization for hydrothermal power plant [17], flower pollination algorithm tuned PI-PD cascade control [18], genetic algorithm (GA)/differential evolution (DE) [19], bat algorithm tuned PD-PID cascade control approach [20], improved stochastic fractal search (SFS) algorithm [21], sine cosine algorithm based PI controller [22], DE tuned PI/PID [23], biogeography based optimization tuned I/PI/PIDF [24], teaching learning based optimization algorithm based 2-degree of freedom (DOF) PID (2DOF-PID) [25], disrupted oppositional based gravitational search algorithm – pattern search based PID [26], symbiotic organism search algorithm tuned PID [27], hybrid SFS – local unimodal sampling (hSFS-LUS) based multi-stage PDF-(1+PI) [28] and imperialist competition algorithm tuned PID controller for PV-thermal and hydrothermal based interconnected power system [29]. A GA-based LFC scheme with stability evaluation under solar, DG, and battery-based distributed energy sources is demonstrated in [7]. A (1+PD)-PID-based cascade control approach for the interconnected power system under RE contributions is briefed in [11]. Kumar and Hote [16] designed a robust PIDD2 controller to mitigate the frequency deviations in the interconnected power system. The authors have chosen Kharitonov's theorem-based worst-case plant section model design. A sliding mode control approach is implemented to design a robust controller [16]. In order to improve the performance of the control scheme, other advanced control approaches based on H-infinity [30], sliding modes [31], fuzzy logic control [32], [33], artificial neural network-based [34], adaptive neuro-fuzzy inference system [35], disturbance observer-based fractional control [36], nonlinear disturbance observer [37], modified tilted control approach [38], delay-dependent control approach including electric vehicles, and constant and varying loads [39], [46] and fractional control approach [40] are discussed. In [33], an intelligent LFC scheme for a standalone MG system is demonstrated. In this, the authors have used an improved IC MPPT scheme to harvest power from PV, and a fuzzy observer-based control approach is chosen for the wind energy conversion system. The obtained results revealed the superior performance of the proposed controller over other considered control approaches. A double-stage controller design is proposed for a hybrid ocean-wind-based maritime MG system [47]. A grasshopper algorithm is used to tune the proposed PI-(1+PD) controller, and the obtained results revealed the enhanced performance of the proposed controller over PID and PID with filter-type controllers. A novel performance index criterion termed a hybrid peak area for the automatic generation control of two area power systems is revealed in [45], and the obtained results are compared with the existing performance indices. A lightning search tuned variable structure control approach for the frequency control of load following a nuclear reactor power system is briefed in [48], and the results are compared with a GA-based variable structure control scheme. An improved gray wolf optimization-based control approach for vision system-based autonomous vehicles is revealed in [49]. A PID controller design for two area power systems via an artificial bee colony is proposed in [50]. A black widow optimization algorithm-based PIDF – (1+I) cascade control approach for the LFC of the MG system is investigated in [51]. This P&O MPPT algorithm is used to harvest maximum obtainable power from PV, and the real-time benchmarking is performed via a modified New England IEEE 39 test bus system. A tilt integral derivative controller for the multi-MG system considering the electric vehicle is presented in [52]. Sensitivity analysis of the proposed control scheme is performed under ±30% of parametric uncertainties. The investigated system performances due to cascade control approaches are worth-appreciating control action in interest. Moreover, selecting an appropriate optimization approach for the LFC design is also challenging for

researchers in this field. However, according to the authors' best knowledge, the system responses depicted in these works have space for further enhancement considering time-domain specifications.

C. MOTIVATION AND CONTRIBUTIONS

Enticed by the structural simplicity of PI and PID controllers and the magnificent performance of cascade and fractional controllers suggested in [11], [40], and [51], the present study preconceives a new fractional cascade controller named (1+PDF)-FOPI, whose performance evaluation has not been investigated so far. The proposed controller has both the property of cascade and fractional order control. As per the literature inspection, many nature-inspired optimizations have been employed for LFC studies. For the optimized search performance, exploitation and exploration are the two vital indices expected to be balanced for the meta-heuristics [15]. A perfect trade-off between exploitation and exploration is obtained with MPA for global optimization. MPA was recently invented metaheuristic proposed by Faramarzi *et al.* [41]. The proposed MPA technique has proved the superior performance over various meta-heuristics such as GA, PSO, cuckoo search (CS), salp swarm algorithm (SSA), gravitational search algorithm (GSA) for various engineering problems such as welded beam design, pressure vessel design, operating fan schedule for demand-controlled ventilation, tension/compression spring design and building energy performance [41]. Hence, tempted by the enhanced performance of the MPA technique, a maiden attempt has been performed to employ it for the LFC of the considered MG system.

Moreover, a stability evaluation of the proposed fractional cascade LFC of the MG system is also performed. The stability assessment approximates the fractional order into its respective entire order using the stability boundary locus (SBL) method [53]. The critical contributions of the work are summarized as follows:

- Design and implement MPA-assisted (1+PDF)-FOPI fractional cascade control scheme for the LFC of renewable-rich MG system.
- To scrutinize the performance of the proposed LFC scheme, five state-of-the-art optimization techniques and PI, FOPID, and PI-PD controllers are considered.
- Eigenvalues-based stability evaluation of the considered MG system employing MPA:(1+PDF)-FOPI controller is performed.
- A New England IEEE-39 test bus system is chosen for the real power system assessment of the proposed controller.

II. SYSTEM DESCRIPTION AND MODELING

A 1.5 MW (1 pu) MG system is considered in this proposed work, as shown in Fig. 1. The power obtained from DG, PV, and WTG are 450 kW, 100 kW, and 750 kW, respectively, whereas UC and flywheel provide 50 kW and 150 kW, respectively.

A. MODELING OF WTG

The rated wind speed (V_w) plays a critical role in the power production from WTG (P_w), and the V_w is dependent on base wind speed (V_{wb}), ramp speed (V_{wr}), gust speed $\left(V_{wg}\right)$ and noise component of wind (V_{wn}) [42]:

$$V_w = V_{wb} + V_{wr} + V_{wg} + V_{wn} \tag{1}$$

The wind model inculcates its essential components as base fluctuation and randomness, which are represented as [43]:

$$V_w = V_{wb} + V_{wn} \tag{2}$$

The V_{wb} is a constant, and its presence is detected when WTG is in operation. Randomness of V_{wb} is expressed by the Heaviside step function as [42]:

$$V_{wb} = C = 7.5H\,(t) + 4.5H\,(t-10) - 2.5H(t-15) \tag{3}$$

In order to consider the practical scenario, variations in V_w is chosen from 2.5 m/s to 12.5 m/s. Moreover, the noise component of V_w is revealed as [43]:

$$V_{wn} = 2\sigma^2 \sum_{i=1}^{n} \sqrt{S_v\,(\omega_i)\,\Delta\omega}\cos(\omega_i t + \varphi_i) \tag{4}$$

where, $\omega_i = \left(i - 1/2\right)\Delta\omega$ and $\varphi_i \approx U(0, 2\pi)$. The noise variation is σ^2 and spectral density critical factor is $\Delta\omega$. The spectral density component $S_v\,(\omega_i)$ is given as [38]:

$$S_v\,(\omega_i) = \frac{2k_n F^2\,|\omega_i|}{\pi^2\left[1 + \left(F_{\omega i}\frac{F_{\omega i}}{\mu\pi}\right)\right]^{4/3}} \tag{5}$$

where, $k_n\mu$ and F denote surface drag coefficient, reference height, and base V_w at turbulence measure. A nonlinear WTG model is considered to harvest the power from unpredictable wind speed. The wind power generation modeling is revealed as [33]:

$$P_W = \frac{1}{2}C_p(\lambda, \beta)\rho A_T V_w^3 \tag{6}$$

$$T_W = \frac{P_W}{\omega_m} \tag{7}$$

where WT angular speed and power output are ω_m and P_W Swept area of the rotor is A_T, air density is ρ, and rotor blade coefficient is C_p that revealed as follows [33]:

$$C_p\,(\lambda, \beta) = C_1 \times \left(\frac{C_2}{\lambda_I} - C_3\beta - C_4\beta^2 - C_5\right) \times e^{-\frac{C_6}{\lambda_I}} + C_7\lambda_T \tag{8}$$

where, C_1 to C_7 are WT's coefficients for fixed and variable speed, the pitch angle is β, and the optimal tip speed ratio is λ_T that demonstrated as [33]:

$$\lambda_T = \lambda_T^{OP} = \frac{\omega_T \times r_T}{V_W} \tag{9}$$

where the radius of the rotor blade is r_T and λ_I is the intermittent tip speed ratio briefed as [33]:

$$\frac{1}{\lambda_I} = \frac{1}{\lambda_T + 0.08\beta} - \frac{0.035}{\beta^3 - 1} \tag{10}$$

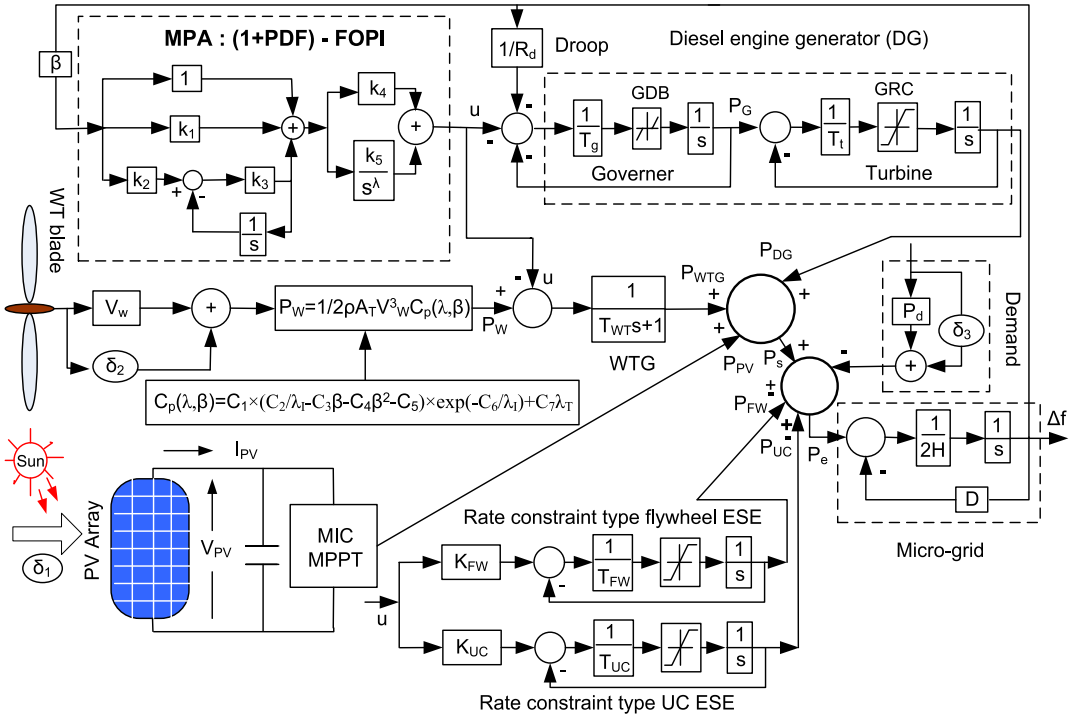

FIGURE 1. Proposed MG system under test.

B. MODELING OF PV SYSTEM

The governing relation of I-V for PV is as follows [44]:

$$I = I_{ph} - I_0 \left\{ e^{\frac{q\left(V_{pv}+R_s I_{pv}\right)}{AKT}} - 1 \right\} - \frac{V_{pv} + R_s I_{pv}}{R_{sh}} \tag{11}$$

where,

$$\begin{cases} I_{ph} = light - generated\ current\ (A) \\ R_{sh}\ and\ R_s = shuntand\ series\ resistances\ (\Omega) \\ T = cell\ temperature\ in\ Kelvin\ (K) \\ I_o = reverse\ saturation\ current\ (A) \\ q = electron\ charge\ \left(1.6022 \times 10^{-19} C\right) \\ I_{pv} = solar\ cell\ output\ current \\ V_{pv} = solar\ cell\ output\ voltage \\ A = the\ p - n\ ideality\ factor \\ K = the\ Boltzman's\ constant (1.38 \times 10^{-23} J/K) \end{cases}$$

The output power of the PV system is briefed as [38]:

$$P_{PV} = \eta S \phi \left\{1 - 0.005\left(T_a + 25\right)\right\} \tag{12}$$

where η is conversion efficacy, S is the measured surface area, ϕ is input insolation on the surface area, and $T_a = 25°\text{C}$ is atmospheric temperature. The solar insolation ϕ is expressed as the heavy step function as [38]:

$$\begin{aligned} \phi = {} & 0.5H\left(t\right) - 0.03H\left(t - 25\right) + 0.3H\left(t - 75\right) \\ & - 0.3H\left(t - 150\right) + \phi_n(t) \end{aligned} \tag{13}$$

where, ϕ_n is in the range (-0.1, 0.1). In this proposed work, the actual PV power through the MIC MPPT scheme is injected into the investigated MG system at the insolation level varying from 400 W/m^2 to 1000 W/m^2 in a ramp variation form. Hence all the nonlinearities of the system are already considered. The obtained maximum power from PV is shown in Fig. 7. The simulation parameters of the PV system are depicted in Table 1.

C. MODELING OF DG

In this proposed work, first order governor model is chosen and revealed as [33]:

$$T_g \dot{P}_G = -P_G - u - \frac{1}{R_d}(\Delta f) \tag{14}$$

where power output and time constant of the governor are P_G and T_g respectively, the control signal is u, and the droop coefficient is R_d. Moreover, the first-order turbine model is chosen and revealed as [33]:

$$T_t \dot{P}_{DG} = -P_{DG} + P_G \tag{15}$$

where power output and time constant of DG are P_{DG} and T_t respectively. The overall open loop transfer function (OLTF) of DG and WTG by assuming other inputs as zero are revealed by (16) and (17) as:

$$\frac{\Delta f}{-u} = \frac{R_d}{R_d\left(T_g s + 1\right)\left(T_t s + 1\right)\left(2Hs + D\right) + 1} \tag{16}$$

$$\frac{\Delta f}{-u} = \frac{1}{\left(\mathrm{T_{WT}} s + 1\right)\left(2Hs + D\right)} \tag{17}$$

where WTG's time constant is $\mathrm{T_{WT}}$, the inertia constant is H, and the MG system's damping coefficient is D.

TABLE 1. Simulation parameters.

System	Specifications						
PV [44]	Maximum power = 100 kW at 1000 W/m^2, number of series connected modules = 5, number of parallel connected modules = 66, number of series connected cell = 96, short circuit current = 5.96 A, open circuit voltage = 64.2 V, maximum power point current = 5.58 A, maximum power point voltage = 54.7 V.						
Wind [33]	$P_W = 750\ kW, \rho = 1.225\ kg.m^3, A_T = 1648\ m^2, r_T =$ 22.9 m, $C_1 = -0.6175, C_2 = 116, C_3 = 0.4, C_4 = 0, C_5 = 5, C_6 = 21,\ C_7 = 0.1405,\ T_{WT} = 0.2\ sec.$						
DG [33]	$P_{DEG} = 100$ kW, $T_g = 0.08\ sec., T_t = 0.4\ sec., R_d = 2$						
Flywheel & UC[33]	$P_{FW} = 150$ kW, $K_{FW} = 0.7, T_{FW} = 0.9\ sec., UC =$ 50 kW, $K_{UC} = 0.01,\ T_{UC} = 0.1\ sec.$						
MG [33]	$H = 0.1, D = 0.015, \beta = 0.3483$, Nominal frequency $= 50\ Hz$						
IEEE 39 [33,45]	Area No.	Unit No.	H	R_d (Hz/MW)	D ($\times 10^{-3}$) (MW/Hz)	T_g (sec.)	T_t (sec.)
	1	1	4.0	3.0	8.33	0.08	0.04
		2	3.5	3.0	8.33	0.08	0.04
		3	2.5	1.8	8.33	0.08	0.04

D. FLYWHEEL AND UC MODELING

The flywheel and UC are utilized as energy storage elements. The linearized model of flywheel and UC are $G_{F1}(s) = \frac{P_{FW}}{P_e}(s) = \frac{K_{FW}}{T_{FW}s+1}$, and $G_{F2}(s) = \frac{P_{UC}}{P_e}(s) = \frac{K_{UC}}{T_{UC}s+1}$, where K_{FW} and K_{UC} are the gains of the flywheel and UC, respectively, T_{FW} and T_{UC} are the time constants of flywheel and UC, respectively. The rate constraint nonlinearities are considered in flywheel and UC [33] and are revealed in Fig. 2.

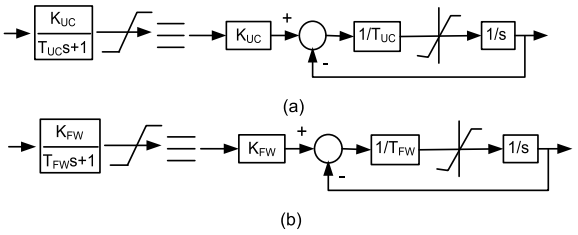

FIGURE 2. Rate constraint model (a) UC and (b) Flywheel.

E. CONSIDERED MICROGRID (MG) MODELING

The description of dynamic modeling of MG system or one-area LFC is revealed in the state space equation model as [46]:

$$\begin{cases} \dot{\bar{x}}(t) = \bar{A}\bar{x}(t) + Bu(t) + \bar{F}\Delta P_d \\ \bar{y}(t) = \bar{C}\bar{x}(t) \end{cases} \tag{18}$$

where, $\bar{x}(t) = \begin{bmatrix} \Delta f & \Delta P_G & \Delta P_v \end{bmatrix}^T$

$$\bar{y}(t) = ACE(area\ control\ error) \tag{19}$$

$$\bar{A} = \begin{bmatrix} \frac{-D}{2H} & \frac{1}{2H} & 0 \\ 0 & \frac{-1}{T_t} & \frac{1}{T_t} \\ \frac{-1}{R_d T_g} & 0 & \frac{-1}{T_g} \end{bmatrix}, \quad \bar{B} = \begin{bmatrix} 0 & 0 & \frac{1}{T_g} \end{bmatrix}^T$$

$$\bar{F} = \begin{bmatrix} \frac{-1}{2H} & 0 & 0 \end{bmatrix}^T, \quad \bar{C} = \begin{bmatrix} \beta & 0 & 0 \end{bmatrix} \tag{20}$$

while considering no tie-line power exchange in MG and β as frequency bias factor, the ACE is as:

$$ACE = \beta\Delta f \tag{21}$$

and

$$CFD = \Delta E(t) = \int_0^t ACE(\tau)d\tau \tag{22}$$

Equations (21) and (22) reveal the integral of $CFD \to 0$ at a steady state. The linearized model of governor valve position due to ACE delay is as:

$$\Delta\dot{P}_v(t) = \frac{-\Delta f(t)}{R_d T_g} - \frac{\Delta P_v(t)}{T_g} - \frac{\Delta E(t - d(t))}{T_g} + \frac{u(t)}{T_g} \tag{23}$$

where, $d(t)$ denotes the system's delay, which is neglected in the present study. In summarized form, (18) is written as:

$$\begin{cases} \dot{x}(t) = Ax(t) + A_d x(t - d(t)) + Bu(t) + F\Delta P_d(t) \\ y(t) = Cx(t) \end{cases} \tag{24}$$

where,

$$x(t) = \begin{bmatrix} \Delta f & \Delta P_G & \Delta P_v \Delta E \end{bmatrix}^T$$

$$A = \begin{bmatrix} \frac{-D}{2H} & \frac{1}{2H} & 0 & 0 \\ 0 & \frac{-1}{T_t} & \frac{1}{T_t} & 0 \\ \frac{-1}{R_d T_g} & 0 & \frac{-1}{T_g} & 0 \\ \beta & 0 & 0 & 0 \end{bmatrix}$$

$$A_d = \begin{bmatrix} 0 & 0 & 0 & 0 \\ 0 & 0 & 0 & 0 \\ 0 & 0 & 0 & \frac{-1}{T_g} \\ 0 & 0 & 0 & 0 \end{bmatrix}$$

$$B = \begin{bmatrix} 0 & 0 & \frac{1}{T_g} & 0 \end{bmatrix}, \quad F = \begin{bmatrix} \frac{-1}{2H} & 0 & 0 & 0 \end{bmatrix},$$

$$C = [1 \quad 0 \quad 0 \quad 1] \tag{25}$$

where Δf is frequency deviation, ΔP_v is valve position and ΔP_d is the change in load demand. The dynamics of the MG system's frequency are demonstrated as [33], [45]:

$$2H\frac{d\Delta f(t)}{dt} = P_{PV} + P_{WTG} + P_{DG} \pm P_{FW}(t) \pm P_{UC}(t) - P_d(t) - D\Delta f(t) \tag{26}$$

The (18) is written in the "s" domain and revealed as:

$$\frac{\Delta f(s)}{P_e(s)} = \frac{1}{2Hs + D} \tag{27}$$

where power error $P_e = P_s - P_d \pm P_{FW} \pm P_{UC}$, and $P_s = P_{PV} + P_{WTG} + P_{DG}$ The power output of the PV, WTG, and DG, respectively. The $\pm P_{FW}$ and $\pm P_{UC}$ reveal the power provided and absorbed by the flywheel and UC, respectively.

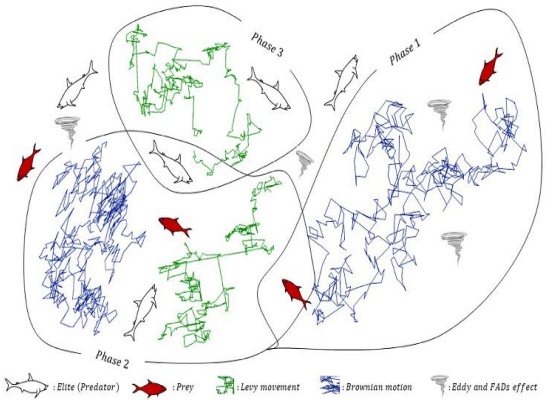

FIGURE 3. Various phases of MPA [41].

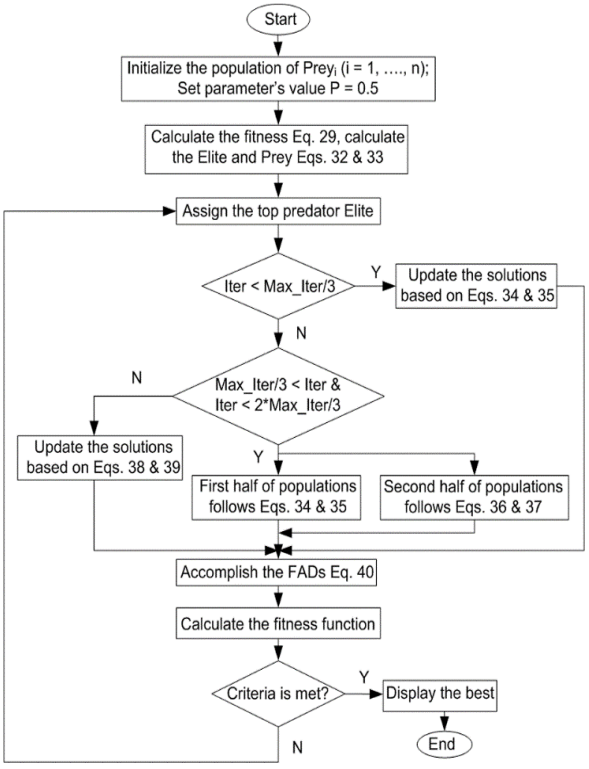

FIGURE 4. Flowchart of MPA.

F. CONTROL STRATEGY

This section reveals the design consideration of the proposed (1+PDF)-FOPI cascade controller used for the droop control in the considered MG system. The output of the (1+PDF) controller is working as the input of the FOPI controller in a series manner; hence, it is considered the cascade control approach. The structure of the (1+PDF)-FOPI controller is shown in Fig. 1 and revealed as:

$$u = \underbrace{\left(1 + k_1\Delta f + k_2 s\frac{k_3}{(s+k_3)}\Delta f\right)}_{(1+\text{PDF})} \times \underbrace{\left(k_4 + \frac{k_5}{s^{\lambda}}\right)}_{\text{FOPI}} \tag{28}$$

where, $k_1 - k_5$ and λ are the parameters of the (1+PDF)-FOPI controller, and u is the controller's output. The total

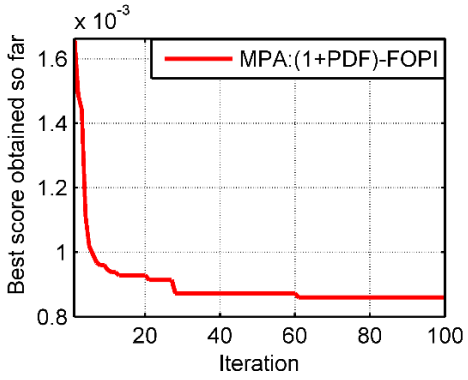

FIGURE 5. Convergence of proposed controller.

tuning parameters of the proposed controller are six. This is the optimization problem and can be reduced by minimizing the objective function (J_s). The different types of objective functions that are used in the LFC of the power system are *IAE*, *ITAE*, *ISE*, and *ITSE*. The *ISE* tuned controller reduces significant errors very fast, but the minor errors remain for a long duration [45]. The *IAE* tuned controller gives a slow dynamic response, and significant deviations remain compared to *ISE* [45]. The controller tuned via *ITAE* and *ITSE* give a dynamic response with less settling time (ST) [45]. The critical shortcoming of *ITAE* and *ITSE* is that the initial dynamic response is slow [45]. Hence, to ramp up the dynamic and steady-state performance (faster convergence with lesser divergence from the final value), an excellent combination is *ISE* and *ITAE*, which is considered in this work and given as:

$$\begin{aligned} J_s &= minimize\,(w_1 \times ISE + w_2 \times ITAE) \\ &= \int_0^{t_s} (w_1 \times |\Delta f|^2 + w_2 \times |\Delta f|.t) \times dt \end{aligned} \tag{29}$$

where, t_s is simulation time, w_1 and w_2 are the weights and chosen as 50% each. The critical aim of this work is to reduce J_s via MPA because reduced J_s provides excellent performance of (1+PDF)-FOPI cascade controller for LFC of considered MG system. Minimize J_s subject to:

$$\begin{aligned} &k_1^{min} \le k_1 \le k_1^{max}, \quad k_2^{min} \le k_2 \le k_2^{max}, \; k_3^{min} \le k_3 \le k_3^{max}, \\ &k_4^{min} \le k_4 \le k_4^{max}, \quad k_5^{min} \le k_5 \le k_5^{max} \text{ and} \\ &\lambda^{min} \le \lambda \le \lambda^{max}. \end{aligned} \tag{30}$$

III. PROPOSED MPA FOR LFC OF CONSIDERED MG SYSTEM

This is a population-based algorithm in which the solution is uniformly distributed as follows [41]:

$$X_o = X_{min} + rand\,(X_{max} - X_{min}) \tag{31}$$

where the lower and upper bounds of variables are X_{max} and X_{min} and $rand[0, 1]$. The fittest predates are in the form of a matrix and searches for prey according to the prey's positional

TABLE 2. Performance evaluation of different schemes.

The constant load of 0.45 pu, without δ_1 and δ_2					
Indices	PSO:(1+PDF)-FOPI	CS:(1+PDF)-FOPI	GSA:(1+PDF)-FOPI	SSA:(1+PDF)-FOPI	Proposed controller
IAE	0.000243	0.000188	0.000158	0.000149	0.000137
ITAE	0.001993	0.001945	0.001647	0.001568	0.001439
ISE	2.34×10^{-7}	7.56×10^{-8}	8.63×10^{-9}	5.98×10^{-9}	4.21×10^{-9}
ITSE	4.22×10^{-8}	4.13×10^{-8}	2.52×10^{-8}	1.89×10^{-8}	1.32×10^{-9}
Max. Δf (Hz)	-0.113	-0.060	-0.059	-0.051	-0.013
ST (sec.)	0.24	0.26	0.18	0.17	0.02

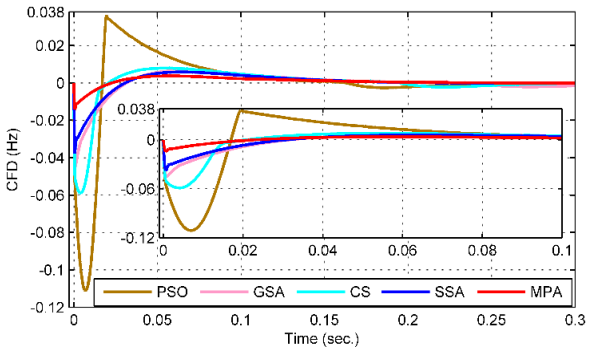

FIGURE 6. Frequency response of controllers under SLP of 45%.

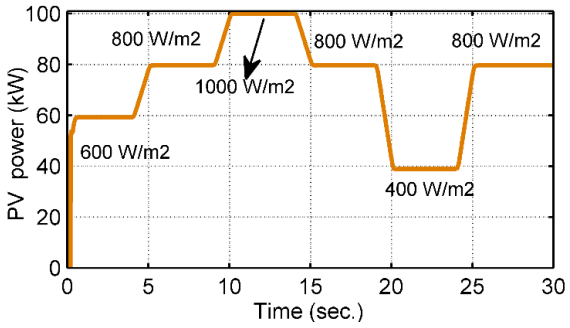

FIGURE 7. Extracted PV power via MIC MPPT scheme.

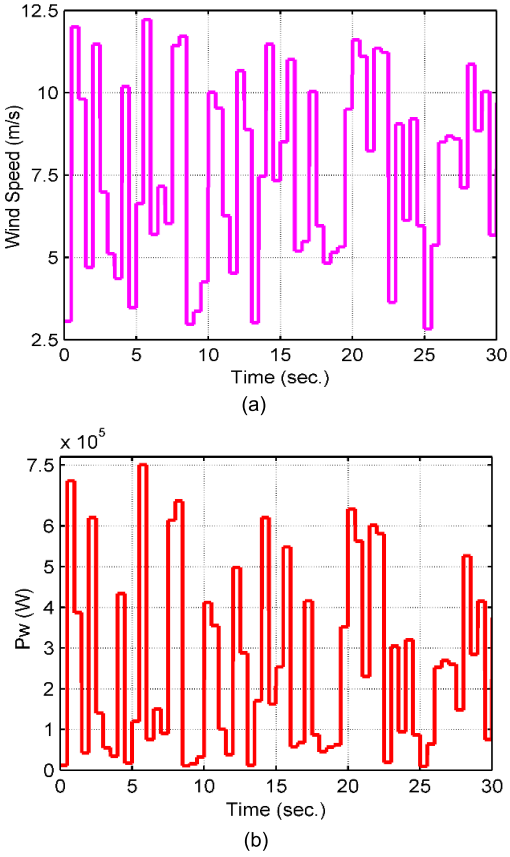

FIGURE 8. (a) stochastic wind speed, and (b) Extracted wind power.

information as [41]:

$$Elite = \begin{bmatrix} X^l_{1,1} & X^l_{1,2} & X^l_{1,d} \\ X^l_{2,1} & X^l_{2,2} & X^l_{2,d} \\ \cdots\cdots\cdots & \cdots\cdots\cdots & \cdots\cdots\cdots \\ \cdots\cdots\cdots & \cdots\cdots\cdots & \cdots\cdots \\ \cdots\cdots\cdots & \cdots\cdots\cdots & \cdots\cdots\cdots \\ X^l_{n,1} & X^l_{n,2} & X^l_{n,d} \end{bmatrix}_{n\times d} \quad (32)$$

where, $\vec{X}^l$ presents the top predator, which replicates n several times to make *Elite* matrix, search agents, and dimensions are n and d. *Elite* is updated if a better predator replaces the top predator. The *Prey* matrix is the same as *Elite* and represented as [41]:

$$Prey = \begin{bmatrix} X_{1,1} & X_{1,2} & X_{1,d} \\ X_{2,1} & X_{2,2} & X_{2,d} \\ \cdots\cdots\cdots & \cdots\cdots\cdots & \cdots\cdots\cdots \\ \cdots\cdots\cdots & \cdots\cdots\cdots & \cdots\cdots\cdots \\ \cdots\cdots\cdots & \cdots\cdots\cdots & \cdots\cdots\cdots \\ X_{n,1} & X_{n,2} & X_{n,d} \end{bmatrix}_{n\times d} \quad (33)$$

When prey and predator move in the same search space, they search for their food. This scenario presents the immediate phase of optimization and exploration that tries to convert into exploitation. Hence, half of the population is designated for exploration, and half is designated for exploitation. In this

TABLE 3. Performance of controller under δ_1, δ_2 and δ_3.

The constant load of 0.55 pu with δ_1 and δ_2					
Schemes	IAE	ITAE	ISE	ITSE	$Max.\Delta f\ (Hz)$
PSO:(1+PDF)-FOPI	0.000261	0.002071	2.470×10^{-7}	4.883×10^{-8}	−0.220
CS:(1+PDF)-FOPI	0.000192	0.002006	8.870×10^{-8}	4.312×10^{-8}	−0.110
GSA:(1+PDF)-FOPI	0.000166	0.001791	9.396×10^{-9}	3.613×10^{-8}	−0.048
SSA:(1+PDF)-FOPI	0.000157	0.001671	7.606×10^{-9}	2.925×10^{-8}	−0.040
MPA: PID	0.008480	0.049832	8.34×10^{-6}	4.883×10^{-7}	−0.300
MPA: FOPID	0.004572	0.008643	3.32×10^{-6}	9.779×10^{-8}	−0.285
MPA: PI-PD	0.000223	0.001651	1.940×10^{-7}	4.425×10^{-8}	−0.147
Proposed controller	0.000146	0.001630	4.970×10^{-9}	6.654×10^{-8}	−0.016
SLP of 0.5 pu, 0.6 pu, and 0.7 pu with δ_1 and δ_2					
PSO:(1+PDF)-FOPI	0.0020770	0.002089	1.345×10^{-8}	1.976×10^{-7}	−0.040
CS:(1+PDF)-FOPI	0.0001668	0.001958	7.736×10^{-9}	5.110×10^{-8}	−0.038
GSA:(1+PDF)-FOPI	0.0001619	0.001756	6.232×10^{-9}	3.779×10^{-8}	−0.025
SSA:(1+PDF)-FOPI	0.0001522	0.001685	6.090×10^{-9}	3.692×10^{-8}	−0.033
MPA: PID	0.0096871	0.009753	6.521×10^{-7}	7.436×10^{-6}	-0.079
MPA: FOPID	0.0064320	0.007143	8.546×10^{-8}	8.631×10^{-7}	-0.062
MPA: PI-PD	0.0001594	0.001621	1.285×10^{-8}	2.891×10^{-8}	-0.022
Proposed controller	0.0001510	0.000169	4.792×10^{-9}	5.185×10^{-9}	−0.008

technique, it is considered that the movement of prey is *Lévy* and the movement of predator are Brownian. The various phases of MPA are revealed in Fig. 3 and presented as:

$$While \frac{1}{3} Max\_Iter < Iter < \frac{2}{3} Max\_Iter$$

For the first half of the population:

$$\overrightarrow{stepsize_i} = \overrightarrow{R}_L \otimes \left(\overrightarrow{Elite_i} - \overrightarrow{R}_L \otimes \overrightarrow{Prey_i}\right) \quad i = 1, \ldots, \frac{n}{2} \tag{34}$$

$$\overrightarrow{Prey_i} = \overrightarrow{Prey_i} + P.\overrightarrow{R} \otimes \overrightarrow{stepsize_i} \tag{35}$$

where, $\overrightarrow{R}_L$ is a vector-based on *Lévy* distribution presenting *Lévy* movement. For the second half of the population, the assumption is as follows [41]:

$$\overrightarrow{stepsize_i} = \overrightarrow{R}_B \otimes \left(\overrightarrow{R}_B \otimes \overrightarrow{Elite_i} - \overrightarrow{Prey_i}\right) \quad i = \frac{n}{2} \ldots n \tag{36}$$

$$\overrightarrow{Prey_i} = \overrightarrow{Elite_i} + P.CF \otimes \overrightarrow{stepsize_i} \tag{37}$$

while $CF = \left(1 - \frac{Iter}{Max\_Iter}\right)^{\left(2\frac{Iter}{Max\_Iter}\right)}$ is an adaptive parameter to control predator movement's step size. The multiplication of $\overrightarrow{R}_B$ furthermore, *Elite* imitates the Brownian movement of the predator, while the updating of the position of prey is based on the predator's Brownian motion.

The last phase of optimization occurs when the movement of a predator is faster than prey and is associated with high exploitation capability. This is represented as:

$$WhileIter > \frac{2}{3} Max\_Iter$$

$$\overrightarrow{stepsize_i} = \overrightarrow{R}_L \otimes \left(\overrightarrow{R}_L \otimes \overrightarrow{Elite_i} - \overrightarrow{Prey_i}\right) \quad i = 1, \ldots, n \tag{38}$$

$$\overrightarrow{Prey_i} = \overrightarrow{Elite_i} + P.CF \otimes \overrightarrow{stepsize_i} \tag{39}$$

TABLE 4. Proposed controller performance under varying MG parameters.

SLP of 0.5 pu, 0.6 pu, and 0.7 pu with δ_1, δ_2 and varying MG parameters				
Parameters	IAE	ITAE	ISE ($\times 10^{-9}$)	ITSE ($\times 10^{-8}$)
$(3 \times 2H, D)$	0.0001535	0.001704	7.826	3.814
$(2H, 3 \times D)$	0.0001520	0.001682	7.735	3.689
$(2H/3, D)$	0.0001475	0.001630	7.428	3.186
$(2H, D/3)$	0.0001521	0.001683	7.737	3.693
$(2H/3, D/3)$	0.0001474	0.001631	7.426	3.193
$(3 \times 2H, 3 \times D)$	0.0001535	0.001703	7.826	3.814

Multiplication of $\overrightarrow{R}_L$ and *Elite* imitates the predator's movement in *Lévy* type while adding step size to *Elite* position imitates the predator's movement for updating of prey position. Another critical factor that affects the MPA is environmental impacts such as fish aggregating devices (*FADs*) effects. *FADs* are considered local-optimal points, and there is a chance to trap these points. The FADs effect is mathematically presented as [41]:

$$\overrightarrow{Prey_i} = \begin{cases} \overrightarrow{Prey_i} + CF\left[\overrightarrow{X}_{min} + \overrightarrow{R} \otimes \left(\overrightarrow{X}_{max} - \overrightarrow{X}_{min}\right)\right] \otimes \overrightarrow{U} \\ \quad if\ r \le FADs \\ \overrightarrow{Prey_i} + [FADs\,(1-r) + r]\left(\overrightarrow{Prey_{r1}} - \overrightarrow{Prey_{r2}}\right) \\ \quad if\ r > FADs \end{cases} \tag{40}$$

where $FADs = 0.2$ is the impact of *FADs* on optimization. Binary vector is $\overrightarrow{U}$ Including an array with one and zero. Vectors containing maximum and minimum bounds are $\overrightarrow{X}_{max}$ and $\overrightarrow{X}_{min}$. Random indexes of the Prey matrix is r_1 and r_2. The flowchart of the MPA is depicted in Fig. 4.

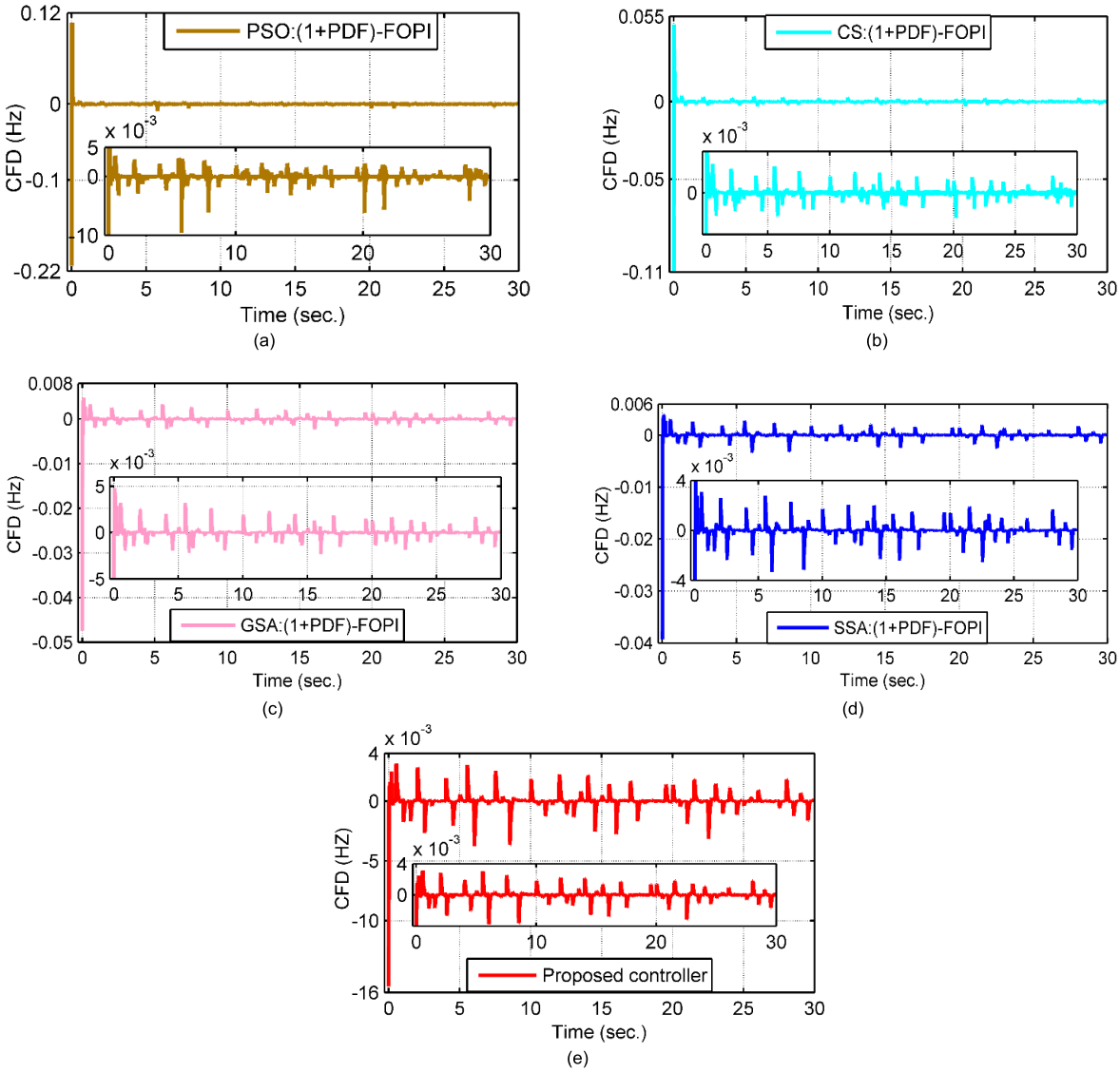

FIGURE 9. (1+PDF)-FOPI controller tuned via (a) PSO (b) CS (c) GSA (d) SSA, and (e) MPA under constant load condition.

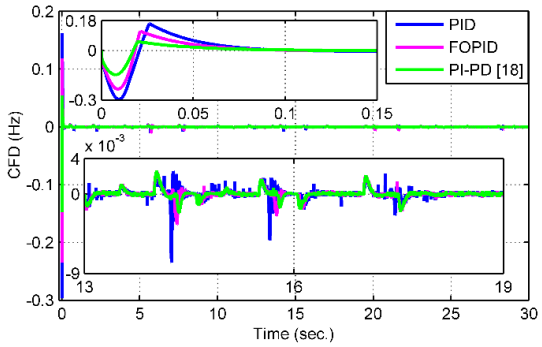

FIGURE 10. MPA-tuned PID, FOPID, and PI-PD controllers under constant load conditions.

IV. RESULTS AND DISCUSSION

A. CONSTANT LOAD CONDITION

The convergence rate of the proposed MPA:(1+PDF)-FOPI controller is shown in Fig. 5. From Fig. 5, the minimum J_s is obtained as 0.000789, and the final convergence is obtained in 60 iterations. In order to investigate the performance of all the applied optimization schemes on the (1+PDF)-FOPI controller, a step load perturbation (SLP) of 45% is given as a load at constant wind speed and constant solar insolation. Hence, an SLP of 45% and without δ_1 (uncertainty in the wind) and δ_2 (uncertainty in solar insolation), The performance of the designed PSO, CS, GSA, SSA and MPA tuned (1+PDF)-FOPI controllers is depicted in Fig. 6 and tabulated in Table 2.

By observing Fig. 6 and Table 2, it can be noted that the maximum Δf is obtained as -0.113 Hz with an ST of 0.24 sec. for PSO:(1+PDF)-FOPI controller. The minimum Δf as -0.013 Hz with a minimum ST of 0.02 sec. is obtained with the proposed MPA:(1+PDF)-FOPI controller. For CS, GSA and SSA tuned (1+PDF)-FOPI controllers, the maximum CFD obtained are -0.06 Hz, -0.059 Hz, and -0.051 Hz with STs are 0.26 sec., 0.18 sec., and 0.17 sec., respectively.

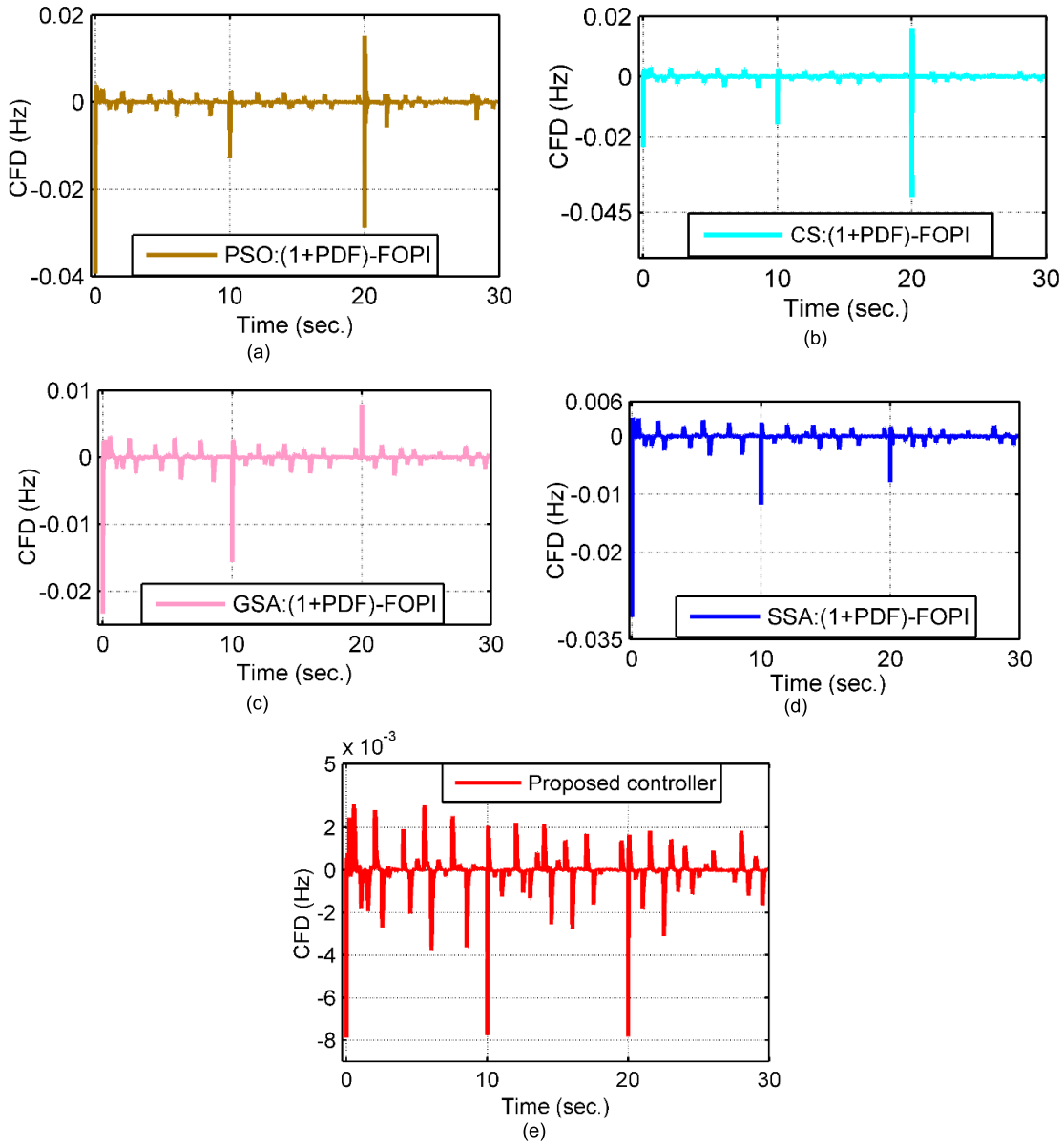

FIGURE 11. (1+PDF)-FOPI controller tuned via (a) PSO (b) CS (c) GSA (d) SSA (e) MPA under varying load condition.

From Table 2, it can be concluded that the error rates are minimum for the proposed controller as IAE(0.000137), ITAE (0.001439), ISE (4.21×10^{-9}) and ITSE (1.32×10^{-9}). So, in this considered state performance, the MPA:(1+PDF)-FOPI controller is superior to other control schemes.

The controller's performance in more practical scenarios by applying a constant SLP of 55% with δ_1 and δ_2 is considered for further analysis. The considered δ_1 is in between 400 W/m^2-1000 W/m^2, and the harvested MPP via MIC MPPT is depicted in Fig. 7. Which shows that the maximum obtained power is 100 kW (0.067 pu) at the maximum insolation of 1000 W/m^2.

The considered δ_2 is in between 2.5 m/s-12.5 m/s, and the extracted MPP via the nonlinear WTG model is depicted in Figs. 8(a)&(b) respectively, the maximum obtained WTG power is 750 kW (0.5 pu). The CFD response of the controllers PSO, CS, GSA, SSA, and MPA tuned (1+PDF)-FOPI is revealed in Figs. 9(a)-(e) respectively. The controller's performance is summarized in Table 3, and from Table 3, the maximum Δf appeared with PSO as -0.22 Hz with IAE (0.000261), ITAE (0.002071), ISE (2.470×10^{-7}), and ITSE (4.883×10^{-8}). For CS, it is -0.11 Hz with IAE (0.000192), ITAE (0.002006), ISE (8.870×10^{-8}), and ITSE (4.312×10^{-8}).

For GSA and SSA, the maximum Δf are -0.048 Hz and -0.40 Hz. The enhanced performance of the proposed MPA:(1+PDF)-FOPI is obtained as -0.016 Hz CFD with IAE (0.000146), ITAE (0.001630), ISE (4.970×10^{-9}), and ITSE

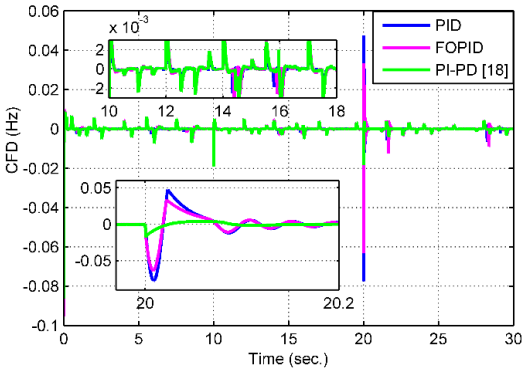

FIGURE 12. MPA-tuned PID, FOPID, and PI-PD controllers under varying load conditions.

(2.701×10^{-8}). In this considered test case, the contribution of all the distributed energy sources with load demand is in Fig. 13(a). Moreover, PID, FOPID, and cascade PI-PD controllers are chosen to assess the proposed controller's superior performance over other traditional controllers, as depicted in Fig. 10. From Fig. 10 and Table 3, the maximum CFD has appeared in MPA: PID controller with valued -0.3 Hz and for MPA: FOPID and MPA: PI-PD controllers CFDs are -0.285 Hz and -0.147 Hz. The maximum error rates appeared for MPA: PID controller compared to MPA: FOPID, PI-PD, and the proposed controller. From the above discussion and Table 3, it can be concluded that the proposed technique surpasses MPA: PID, MPA: FOPID, and MPA: PI-PD controllers under transient and steady-state performance.

B. VARYING LOAD CONDITION

A varying load demand as SLP of 50%, 60%, and 70% with δ_1 and δ_2 are considered for benchmarking the (1+PDF)-FOPI controller tuned via PSO, CS, GSA, SSA, and MPA. The response of CFD for all the designed control schemes are revealed in Figs. 11(a)-(e), and the performance is summarized in Table 3. The maximum CFD has appeared with PSO as -0.04 Hz with IAE (0.0020770), ITAE (0.002089), ISE (1.345×10^{-8}), and ITSE (1.976×10^{-7}) With CS tuned (1+PDF)-FOPI controller, the maximum CFD is -0.038 Hz with IAE (0.0001668), ITAE (0.001958), ISE (7.736×10^{-9}), and ITSE (5.110×10^{-8}). With GSA and SSA, the maximum CFDs are -0.025 Hz and -0.033 Hz, respectively; with the proposed MPA:(1+PDF)-FOPI controller, the maximum CFD is minimum and valued as -0.08 Hz with IAE (0.0001510), and ITAE (0.000169), ISE (4.792×10^{-9}), and ITSE (5.185×10^{-9}). The comparative analysis of the MPA: PID, MPA: FOPID, MPA: PI-PD, and proposed controllers are tabulated in Table 3 and depicted in Figs 11(e) and 12. The maximum CFD is obtained for MPA: PID with a value of -0.079 Hz, whereas for MPA: FOPID and MPA: PI-PD are -0.062 Hz and -0.022 Hz. The error rates are higher for MPA: PID, MPA: FOPID, and MPA: PI-PD controllers

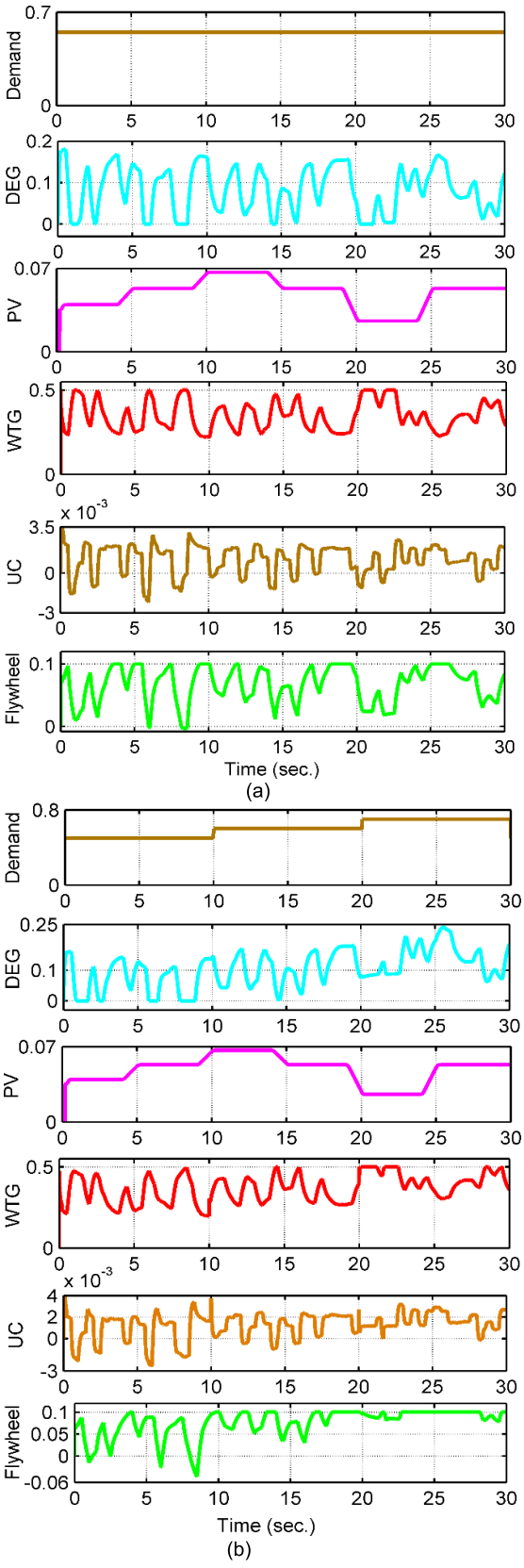

FIGURE 13. Distributed generations contributions via proposed controller, (a) constant load condition, (b) Varying load condition.

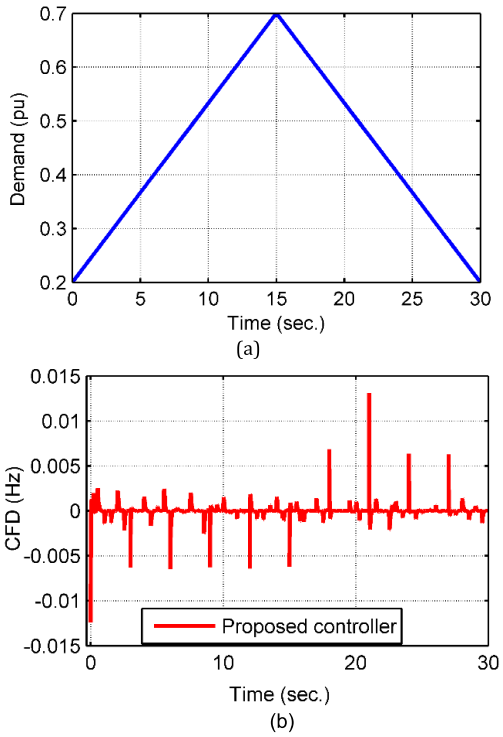

FIGURE 14. (a) load variations, and (b) CFD for the proposed controller.

compared to the proposed control scheme. Hence, it can be concluded that the proposed controller surpasses the other designed controller for the considered test case.

To assess the robustness performance of the proposed controller, parametric variations are considered. The various components of parametric uncertainties will primarily affect the parameters of the MG system. Hence, a large perturbation order of 300% change in 2H and 300% change in D is considered for the robustness evaluation of the proposed controller. In this scenario, the controller's performance in terms of the error rates is summarized in Table 4, which is reasonably satisfactory. In order to investigate the robustness analysis of the proposed controller in a harsh situation, a rigorous load variation is also considered, as depicted in Fig. 14(a), and the performance of the MPA:(1+PDF)-FOPI controller is revealed in Fig. 14(b). Considering the challenging scenario, the performance of the proposed controller is entirely satisfactory, with a maximum CFD of −0.014 Hz, which is under the permissible limit of the IEEE standard.

C. STABILITY EVALUATION

In order to boost the dynamic performance of an LFC technique, it is required to have enough stability. Various schemes

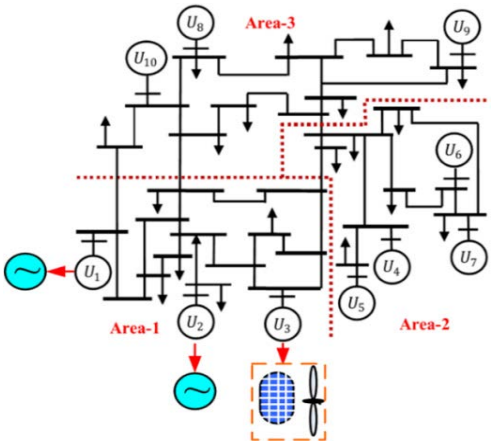

FIGURE 15. Modified New England IEEE-39 bus system [44].

are available to assess the stability of a system and the eigenvalues-based stability approach is one of them. To obtain the eigenvalues, first, the fractional order term is converted into an absolute order term using the stability boundary locus (SBL) scheme [53]. The controller TF is revealed as:

$$C(s) = \left(1 + k_1 + \frac{k_2 k_3 s}{(s+k_3)}\right)\left(k_4 + \frac{k_5}{s^{\lambda}}\right) = \left(1 + 823.51 + \frac{189.3965}{(s+100)}\right)\left(17.95 + \frac{405.19}{s^{0.6}}\right) \tag{41}$$

where, $s^{0.6} = \frac{34470s^4+56770s^3+12680s^2+405.6s+1}{6300s^4+5493s^3+38800s^2+4074s+52.66}$.

The complete closed loop TF of the considered MG system employing the proposed fractional cascade LFC is evaluated using [54] and revealed by as in (42), shown at the bottom of the page. The obtained eigenvalues for MPA:(1+PDF)-FOPI controlled considered MG system are as follows: $-100.0000 + 0.0000i$, $-13.0689 + 0.0000i$, $-10.0000 + 0.0000i$, $-5.0000 + 0.0000i$, $-1.0031 + 2.2696i$, $-1.0031 - 2.2696i$, $-1.3880 + 0.0000i$, $-1.1111 + 0.0000i$, $-0.2211 + 0.0000i$, $-0.0750 + 0.0000i$, $-0.0352 + 0.0000i$, $-0.0027 + 0.0000i$. The evaluated eigenvalues show that the proposed MPA:(1+PDF)-FOPI fractional cascade control scheme can stabilize the considered MG system.

D. IMPLEMENTATION OF PROPOSED CONTROL SCHEME ON REAL POWER SYSTEM

To benchmark, the proposed MPA:(1+PDF)-FOPI fractional cascade controller on a real power system, a modified New England IEEE-39 bus system, is considered. The ten reheat-type thermal generators in three areas are present in the

$$G(s) = \frac{5.316\times10^5 s^{10}+6.478\times10^7 s^9+2.052\times10^9 s^8+2.632\times10^{10} s^7+1.564\times10^{11} s^6+4.566\times10^{11} s^5+6.978\times10^{11} s^4+4.449\times10^{11} s^3+1.08\times10^{11} s^2+8.243\times10^9 s+1.008\times10^8}{0.7942s^{12}+105.6s^{11}+2928s^{10}+3.326\times10^4 s^9+1.858\times10^5 s^8+5.939\times10^5 s^7+1.237\times10^6 s^6+1.516\times10^6 s^5+9.064\times10^5 s^4+1.973\times10^5 s^3+1.45\times10^4 s^2+324.9s+0.7725} \tag{42}$$

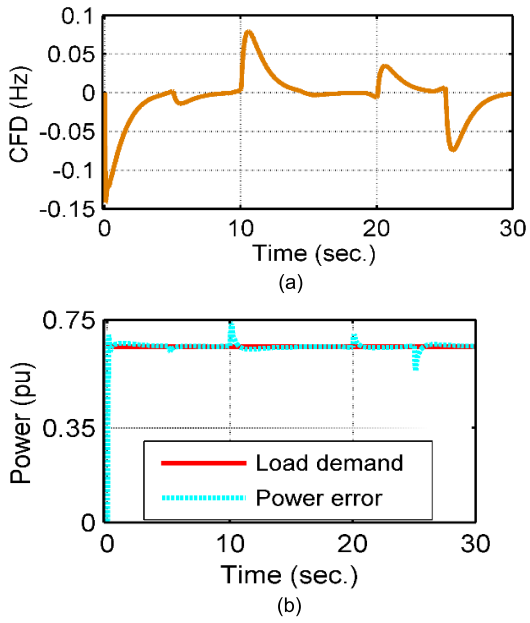

FIGURE 16. Response of proposed controller for area-1 (constant demand) (a) power (b) CFD.

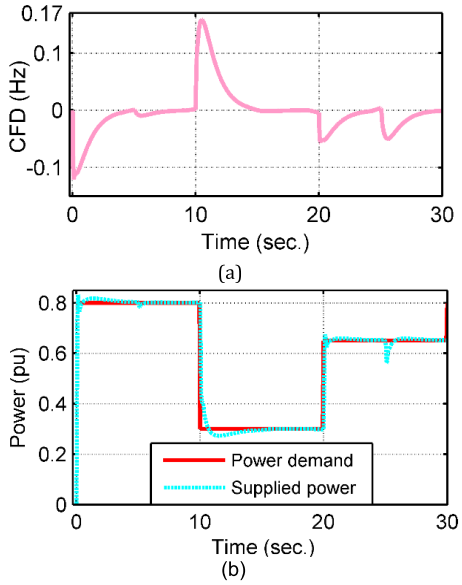

FIGURE 17. Response of proposed controller for area-1 (varying demand) (a) power, and (b) CFD.

standard IEEE-39 bus system [45]. In this work, out of three areas, only one area, i.e., area 1, is chosen to assess the proposed control scheme. The modification is done in area 1, where one conventional generator is replaced by the solar and wind as generating units and a flywheel as a storage unit. The considered modified IEEE-39 bus system is depicted in Fig. 15. The related simulation parameters are given in Table 1.

The effect of GRC nonlinearity is also incorporated in this study. The frequency response, supply, and demand power for SLP 65% pu are depicted in Fig. 16 (a) and (b). Maximum $\boldsymbol{\Delta f}$ is obtained in the order of -0.148 Hz, which is reasonably satisfactory and within the permissible range. The performance is tested by employing the varying power demand of SLP 80%, 30%, and 65%, and responses are depicted in Figs. 17(a) and (b); with varying power demand, the maximum obtained $\boldsymbol{\Delta f}$ is $+0.169$ Hz, which is in the permissible frequency range. The idea of the proposed MG system may be implemented for the places which are not accessible to the conventional grid but enriched with RE sources, for rural electrification, hospitals, agricultural fields, etc. The proposed control scheme may be applied to control interconnected power systems and hybrid electric vehicles.

V. CONCLUSION

The study made in this paper has been directed toward a novel MPA:(1+PDF)-FOPI fractional cascade LFC for a 1.5 MW standalone MG system. The maximum PV power is successfully harvested via a modified IC MPPT technique, and the optimal power is extracted from the wind via a designed nonlinear WTG model. The results of the proposed controller are vividly compared with four state-of-the-art optimization techniques, PSO, CS, GSA, SSA, and three controllers, PID, FOPID, and cascade PI-PD. The obtained performance indices and maximum CFD show the effectiveness and superiority of the proposed LFC scheme over the other designed control schemes. For the robustness assessment of the proposed LFC scheme, huge parametric uncertainties are considered in the MG system's parameters, and rigorous load demand in triangular format is also considered. Under the worst situation, the maximum frequency deviation is -0.016 Hz, which is under the permissible limit. The controller has performed well, and CFD is under the permissible limit of the IEEE standard. Eigenvalues-based stability analysis shows the stable performance of the proposed control scheme. Finally, a modified New England IEEE-39 test bus system is successfully implemented to assess the proposed control scheme's actual power system implementation in an off-line scenario. This work's future scope may focus on designing of intelligent control scheme for renewable-rich multi-area power systems.

REFERENCES

[1] M. Ramesh, A. K. Yadav, and P. K. Pathak, "An extensive review on load frequency control of solar-wind based hybrid renewable energy systems," *Energy Sources A, Recovery, Utilization, Environ. Effects*, pp. 1–25, Jun. 2021.

[2] Z. Zhuo, N. Zhang, J. Yang, C. Kang, C. Smith, M. J. O'Malley, and B. Kroposki, "Transmission expansion planning test system for AC/DC hybrid grid with high variable renewable energy penetration," *IEEE Trans. Power Syst.*, vol. 35, no. 4, pp. 2597–2608, Jul. 2020.

[3] P. K. Pathak, A. K. Yadav, and P. A. Alvi, "A state-of-the-art review on shading mitigation techniques in solar photovoltaics via meta-heuristic approach," *Neural Comput. Appl.*, vol. 34, no. 1, pp. 171–209, Jan. 2022.

[4] S. M. Sousa, L. S. Gusman, T. A. S. Lopes, H. A. Pereira, and J. M. S. Callegari, "MPPT algorithm in single loop current-mode control applied to DC–DC converters with input current source characteristics," *Int. J. Electr Power Energy Syst.*, vol. 138, Jun. 2022, Art. no. 107909.

[5] P. K. Pathak, A. K. Yadav, and P. A. Alvi, "Advanced solar MPPT techniques under uniform and non-uniform irradiance: A comprehensive review," *J. Sol. Energy Eng.*, vol. 142, no. 4, Aug. 2020, Art. no. 040801.

[6] C. Huang, F. Li, and Z. Jin, "Maximum power point tracking strategy for large-scale wind generation systems considering wind turbine dynamics," *IEEE Trans. Ind. Electron.*, vol. 62, no. 4, pp. 2530–2539, Apr. 2015.

[7] P. K. Pathak, S. Padmanaban, A. K. Yadav, P. A. Alvi, and B. Khan, "Modified incremental conductance MPPT algorithm for SPV-based grid-tied and stand-alone systems," *IET Gener., Transmiss. Distrib.*, vol. 16, no. 4, pp. 776–791, Feb. 2022.

[8] P. Mercier, R. Cherkaoui, and A. Oudalov, "Optimizing a battery energy storage system for frequency control application in an isolated power system," *IEEE Trans. Power Syst.*, vol. 24, no. 3, pp. 1469–1477, Aug. 2009.

[9] M. Ma, C. Zhang, X. Liu, and H. Chen, "Distributed model predictive load frequency control of the multi-area power system after deregulation," *IEEE Trans. Ind. Electron.*, vol. 64, no. 6, pp. 5129–5139, Jun. 2017.

[10] F. Liu, Y. Li, Y. Cao, J. She, and M. Wu, "A two-layer active disturbance rejection controller design for load frequency control of interconnected power system," *IEEE Trans. Power Syst.*, vol. 31, no. 4, pp. 3320–3321, Jul. 2016.

[11] E. Çelik, N. Öztürk, Y. Arya, and C. Ocak, "(1+PD)-PID cascade controller design for performance betterment of load frequency control in diverse electric power systems," *Neural Comput. Appl.*, vol. 33, pp. 15433–15456, Jun. 2021.

[12] E. S. Ali and S. M. Abd-Elazim, "Bacteria foraging optimization algorithm based load frequency controller for interconnected power system," *Int. J. Elect. Power Energy Syst.*, vol. 33, no. 3, pp. 633–638, 2011.

[13] S. Panda, B. Mohanty, and P. K. Hota, "Hybrid BFOA—PSO algorithm for automatic generation control of linear and nonlinear interconnected power systems," *Appl. Soft Comput.*, vol. 13, no. 12, pp. 4718–4730, 2013.

[14] M. Farahani, S. Ganjefar, and M. Alizadeh, "PID controller adjustment using chaotic optimisation algorithm for multi-area load frequency control," *IET Control Theory Appl.*, vol. 6, no. 13, pp. 1984–1992, 2012.

[15] S. M. Abd-Elazim and E. S. Ali, "Load frequency controller design of a two-area system composing of PV grid and thermal generator via firefly algorithm," *Neural Comput. Appl.*, vol. 30, no. 2, pp. 607–616, Jul. 2018.

[16] M. Kumar and Y. V. Hote, "Robust PIDD2 controller design for perturbed load frequency control of an interconnected time-delayed power systems," *IEEE Trans. Control Syst. Technol.*, vol. 29, no. 6, pp. 2662–2669, Nov. 2021.

[17] M. Omar, M. Soliman, A. A. Hany, and F. Bendary, "Optimal tuning of PID controllers for hydrothermal load frequency control using ant colony optimization," *Int. J. Electr. Eng. Inform.*, vol. 5, no. 3, pp. 340–348, 2013.

[18] S. Padhy and S. Panda, "A hybrid stochastic fractal search and pattern search technique based cascade PI-PD controller for automatic generation control of multi-source power systems in presence of plug in electric vehicles," *CAAI Trans. Intell. Technol.*, vol. 2, no. 1, pp. 12–25, 2017.

[19] S. K. Sahoo, "Control techniques in AC, DC, and hybrid AC–DC microgrid: A review," *IEEE J. Emerg. Sel. Topics Power Electron.*, vol. 6, no. 2, pp. 738–759, Jun. 2018.

[20] P. Dash, L. C. Saikia, and N. Sinha, "Automatic generation control of multi area thermal system using Bat algorithm optimized PD–PID cascade controller," *Int. J. Elect. Power Energy Syst.*, vol. 68, pp. 364–372, Jun. 2015.

[21] E. Çelik, "Improved stochastic fractal search algorithm and modified cost function for automatic generation control of interconnected electric power systems," *Eng. Appl. Artif. Intell.*, vol. 88, Feb. 2020, Art. no. 103407.

[22] P. Satapathy, M. K. Debnath, and P. K. Mohanty, "Design of PD-PID controller with double derivative filter for frequency regulation," in *Proc. 2nd IEEE Int. Conf. Power Electron., Intell. Control Energy Syst. (ICPEICES)*, Oct. 2018, pp. 1142–1147.

[23] P. K. Hota and B. Mohanty, "Automatic generation control of multi source power generation under deregulated environment," *Int. J. Electr. Power Energy Syst.*, vol. 75, pp. 205–214, Feb. 2016.

[24] A. Rahman, L. C. Saikia, and N. Sinha, "Automatic generation control of an interconnected two-area hybrid thermal system considering dish-stirling solar thermal and wind turbine system," *Renew. Energy*, vol. 105, pp. 41–54, May 2017.

[25] R. K. Sahu, S. Panda, U. K. Rout, and D. K. Sahoo, "Teaching learning based optimization algorithm for automatic generation control of power system using 2-DOF PID controller," *Int. J. Electr. Power Energy Syst.*, vol. 77, pp. 287–301, May 2016.

[26] R. K. Khadanga and A. Kumar, "Hybrid adaptive 'gbest'-guided gravitational search and pattern search algorithm for automatic generation control of multi-area power system," *IET Gener., Transmiss. Distrib.*, vol. 11, no. 13, pp. 3257–3267, 2017.

[27] D. Guha, P. K. Roy, and S. Banerjee, "Symbiotic organism search algorithm applied to load frequency control of multi-area power system," *Energy Syst.*, vol. 9, no. 2, pp. 439–468, May 2018.

[28] R. Sivalingam, S. Chinnamuthu, and S. S. Dash, "A hybrid stochastic fractal search and local unimodal sampling based multistage PDF plus (1+PI) controller for automatic generation control of power systems," *J. Franklin Inst.*, vol. 354, no. 12, pp. 4762–4783, 2017.

[29] Y. Arya, "AGC of PV-thermal and hydro-thermal power systems using CES and a new multi-stage FPIDF-(1+PI) controller," *Renew. Energy*, vol. 134, pp. 796–806, Apr. 2019.

[30] A. D. Rosaline and U. Somarajan, "Structured H-infinity controller for an uncertain deregulated power system," *IEEE Trans. Ind. Appl.*, vol. 55, no. 1, pp. 892–906, Jan. 2019.

[31] C. Mu, Y. Tang, and H. He, "Improved sliding mode design for load frequency control of power system integrated an adaptive learning strategy," *IEEE Trans. Ind. Electron.*, vol. 64, no. 8, pp. 6742–6751, Aug. 2017.

[32] H. A. Yousef, K. Al-Kharusi, M. H. Albadi, and N. Hosseinzadeh, "Load frequency control of a multi-area power system: An adaptive fuzzy logic approach," *IEEE Trans. Power Syst.*, vol. 29, no. 4, pp. 1822–1830, Jul. 2014.

[33] M. Ramesh, A. K. Yadav, and P. K. Pathak, "Intelligent adaptive LFC via power flow management of integrated standalone micro-grid system," *ISA Trans.*, vol. 112, pp. 234–250, Jun. 2021.

[34] D. Qian and G. Fan, "Neural-network-based terminal sliding mode control for frequency stabilization of renewable power systems," *IEEE/CAA J. Autom. Sinica*, vol. 5, no. 3, pp. 706–717, May 2018.

[35] K. R. Reddy and S. Meikandasivam, "Load flattening and voltage regulation using plug-in electric vehicle's storage capacity with vehicle prioritization using ANFIS," *IEEE Trans. Sustain. Energy*, vol. 11, no. 1, pp. 260–270, Jan. 2020.

[36] F. Yang, X. Shao, S. M. Muyeen, D. Li, S. Lin, and C. Fang, "Disturbance observer based fractional-order integral sliding mode frequency control strategy for interconnected power system," *IEEE Trans. Power Syst.*, vol. 36, no. 6, pp. 5832–5922, Nov. 2021.

[37] K. Liao and Y. Xu, "A robust load frequency control scheme for power systems based on second-order sliding mode and extended disturbance observer," *IEEE Trans. Ind. Informat.*, vol. 14, no. 7, pp. 3076–3086, Jul. 2018.

[38] K. Singh, M. Amir, F. Ahmad, and M. A. Khan, "An integral tilt derivative control strategy for frequency control in multimicrogrid system," *IEEE Syst. J.*, vol. 15, no. 1, pp. 1477–1488, Mar. 2021.

[39] H.-B. Zeng, S.-J. Zhou, X.-M. Zhang, and W. Wang, "Delay-dependent stability analysis of load frequency control systems with electric vehicles," *IEEE Trans. Cybern.*, early access, Jan. 25, 2022, doi: 10.1109/TCYB.2022.3140463.

[40] I. Pan and S. Das, "Fractional order AGC for distributed energy resources using robust optimization," *IEEE Trans. Smart Grid*, vol. 7, no. 5, pp. 2175–2186, Sep. 2016.

[41] A. Faramarzi, M. Heidarinejad, S. Mirjalili, and A. H. Gandomi, "Marine predators algorithm: A nature-inspired metaheuristic," *Expert Syst. Appl.*, vol. 152, Aug. 2020, Art. no. 113377.

[42] P. Anderson and A. Bose, "Stability simulation of wind turbine systems," *IEEE Trans. Power App. Syst.*, vol. PAS-102, no. 12, pp. 3791–3795, Dec. 1983.

[43] D.-J. Lee and L. Wang, "Small-signal stability analysis of an autonomous hybrid renewable energy power generation/energy storage system. Part I: Time-domain simulations," *IEEE Trans. Energy Convers.*, vol. 23, no. 1, pp. 311–320, Mar. 2008.

[44] P. K. Pathak and A. K. Yadav, "Design of battery charging circuit through intelligent MPPT using SPV system," *Sol. Energy*, vol. 178, pp. 79–89, Jan. 2019.

[45] N. Pathak and Z. Hu, "Hybrid-peak-area-based performance index criteria for AGC of multi-area power systems," *IEEE Trans. Ind. Informat.*, vol. 15, no. 11, pp. 5792–5802, Nov. 2019.

[46] L. Jiang, W. Yao, Q. H. Wu, J. Y. Wen, and S. J. Cheng, "Delay-dependent stability for load frequency control with constant and time-varying delays," *IEEE Trans. Power Syst.*, vol. 27, no. 2, pp. 932–941, May 2012.

[47] A. Latif, S. M. S. Hussain, D. C. Das, and T. S. Ustun, "Double stage controller optimization for load frequency stabilization in hybrid wind-ocean wave energy based maritime microgrid system," *Appl. Energy*, vol. 282, Jan. 2021, Art. no. 116171.

[48] M. Elsisi and H. Abdelfattah, "New design of variable structure control based on lightning search algorithm for nuclear reactor power system considering load-following operation," *Nucl. Eng. Technol.*, vol. 52, no. 3, pp. 544–551, Mar. 2020.
[49] M. Elsisi, "Improved grey wolf optimizer based on opposition and quasi learning approaches for optimization: Case study autonomous vehicle including vision system," *Artif. Intell. Rev.*, pp. 1–24, Jan. 2022.
[50] M. Elsisi, M. Soliman, M. A. S. Aboelela, and W. Mansour, "ABC based design of PID controller for two area load frequency control with nonlinearities," *TELKOMNIKA Indonesian J. Elect. Eng.*, vol. 16, no. 1, pp. 58–64, 2015.
[51] P. K. Pathak, A. K. Yadav, A. Shastri, and P. A. Alvi, "BWOA assisted PIDF-(1+I) controller for intelligent load frequency management of standalone micro-grid," *ISA Trans.*, pp. 1–15, Jun. 2022.
[52] B. Khokhar, S. Dahiya, and K. P. S. Parmar, "Load frequency control of a multi-microgrid system incorporating electric vehicles," *Electric Power Compon. Syst.*, vol. 49, nos. 9–10, pp. 867–883, Jun. 2021.
[53] F. N. Deniz, B. B. Alagoz, N. Tan, and D. P. Atherton, "An integer order approximation method based on stability boundary locus for fractional order derivative/integrator operators," *ISA Trans.*, vol. 62, pp. 154–163, May 2016.
[54] A. X. R. Irudayaraj, N. I. A. Wahab, M. G. Umamaheswari, M. A. M. Radzi, N. B. Sulaiman, V. Eerasamy, and R. Ramachandran, "A Matignon's theorem based stability analysis of hybrid power system for automatic load frequency control using atom search optimized FOPID controller," *IEEE Access*, vol. 8, pp. 168751–168772, 2020.

PAWAN KUMAR PATHAK received the B.Tech. degree in electrical and electronics engineering from GBTU, Lucknow, India, in 2013, the M.E. degree (Hons.) in power electronics from RGPV Bhopal, India, in 2015, and the Ph.D. degree in electrical engineering from Banasthali Vidyapith, Rajasthan, India, in 2021. He is currently working as an Assistant Professor with the School of Automation, Banasthali Vidyapith. He has more than seven years of teaching and research experience and published more than 20 research papers in journals and conferences of repute. His research interests include renewable energy, load frequency control, battery charger, electric vehicles, cyber-physical power systems, intelligent control, and meta-heuristics.

ANIL KUMAR YADAV (Senior Member, IEEE) received the B.Tech. degree in electronics and instrumentation engineering from Uttar Pradesh Technical University, Lucknow, India, in 2007, and the M.Tech. and Ph.D. degrees in instrumentation and control engineering from the University of Delhi, Delhi, India, in 2010 and 2017, respectively. He is currently working as an Assistant Professor with the Department of Electrical Engineering, NIT Hamirpur, Hamirpur, Himachal Pradesh, India. He is a member of the Institution of Engineers, India. He has 14 years of teaching and research experience and published more than 60 research papers in journals and conferences of repute. His research interests include renewable energy, hybrid systems, and nonlinear and intelligent control.

SANJEEVIKUMAR PADMANABAN (Senior Member, IEEE) received the Ph.D. degree in electrical engineering from the University of Bologna, Bologna, Italy, in 2012.

He was an Associate Professor at VIT University, from 2012 to 2013. In 2013, he joined the National Institute of Technology, India, as a Faculty Member. In 2014, he was invited as a Visiting Researcher at the Department of Electrical Engineering, Qatar University, Doha, Qatar, funded by the Qatar National Research Foundation (Government of Qatar). He continued his research activities with the Dublin Institute of Technology, Dublin, Ireland, in 2014. Further, he worked as an Associate Professor with the Department of Electrical and Electronics Engineering, University of Johannesburg, Johannesburg, South Africa, from 2016 to 2018. From March 2018 to February 2021, he was an Assistant Professor with the Department of Energy Technology, Aalborg University, Esbjerg, Denmark. Since March 2021, he has been an Associate Professor with the CTIF Global Capsule (CGC) Laboratory, Department of Business Development and Technology, Aarhus University, Herning, Denmark. He is currently a Full Professor in electrical power engineering with the Department of Electrical Engineering, Information Technology, and Cybernetics, University of South-Eastern Norway, Norway. He has authored over more than 500 scientific papers.

Dr. Padmanaban received the Best Paper cum Most Excellence Research Paper Award from IET-SEISCON'13, IET-CEAT'16, IEEE-EECSI'19, IEEE-CENCON'19, and five best paper awards from ETAEERE'16 sponsored Lecture Notes in book *Electrical Engineering* (Springer). He is a fellow of the Institution of Engineers, India, the Institution of Electronics and Telecommunication Engineers, India, and the Institution of Engineering and Technology, U.K. He received a Lifetime Achievement Award from Marquis Who's Who—USA 2017 for contributing to power electronics and renewable energy research. Since 2019, he has been listed among the world's top 2 scientists by Stanford University, USA. He is an Editor/an Associate Editor/an Editorial Board for refereed journals, in particular the IEEE Systems Journal, IEEE Transaction on Industry Applications, IEEE Access, *IET Power Electronics*, *IET Electronics Letters*, and *International Transactions on Electrical Energy Systems* (Wiley), a Subject Editorial Board Member of *Energy Sources*, *Energies* journal, MDPI, and the Subject Editor of the *IET Renewable Power Generation*, *IET Generation, Transmission and Distribution*, and *FACETS* journal (Canada).

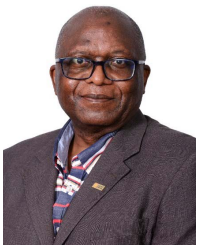

INNOCENT KAMWA (Fellow, IEEE) received the Ph.D. degree in electrical engineering from Laval University, in 1989. He is currently a Full Professor with the Department of Electrical Engineering and the Tier 1 Canada Research Chair in decentralized sustainable electricity grids for smart communities at Laval University. He was previously a Researcher at Hydro-Québec's Research Institute, specializing in the dynamic performance and control of power systems. He was also the Chief Scientist for Hydro-Québec's Smart Grid Innovation Program and an international consultant in power grid simulation and network stability. He is a fellow of the Canadian Academy of Engineering and the IEEE for his innovations in power system control. He was a recipient of the 2019 IEEE Charles Proteus Steinmetz Award and the Charles Concordia Award. He was the Editor-in-Chief of the *IET Generation, Transmission, and Distribution*. He is currently the Editor-in-Chief of the *IEEE Power and Energy Magazine* and an Associate Editor of the IEEE Transactions on Power Systems.